



Engineering Multifunctional RNAi Nanomedicine To Concurrently Target Cancer Hallmarks for Combinatorial Therapy

Yanlan Liu,* Xiaoyuan Ji, Winnie W. L. Tong, Diana Askhatova, Tingyuan Yang, Hongwei Cheng, Yuzhuo Wang, and Jinjun Shi*

Abstract: Cancer hallmarks allow the complexity and heterogeneity of tumor biology to be better understood, leading to the discovery of various promising targets for cancer therapy. An amorphous iron oxide nanoparticle (NP)-based RNAi strategy is developed to co-target two cancer hallmarks. The NP technology can modulate the glycolysis pathway by silencing MCT4 to induce tumor cell acidosis, and concurrently exacerbate oxidative stress in tumor cells via the Fenton-like reaction. This strategy has the following features for systemic siRNA delivery: 1) siRNA encapsulation within NPs for improving systemic stability; 2) effective endosomal escape through osmotic pressure and/or endosomal membrane oxidation; 3) small size for enhancing tumor tissue penetration; and 4) triple functions (RNAi, Fenton-like reaction, and MRI) for combinatorial therapy and in vivo tracking.

Hypoxia is recognized as a fundamentally important feature of solid tumors and is at the heart of cancer hallmarks.^[1] Under hypoxia, metabolic pathways of cancer cells may therefore be rewired in such a way that balances biosynthetic processes with rapid and large amounts of ATP production to support cell proliferation,^[2] a phenomenon referred to as aerobic glycolysis or the “Warburg effect” that is uniquely observed in primary and metastatic tumors.^[3] The high rate of glycolysis is associated with excessive generation of lactic acid,^[4] which leads to the upregulation of monocarboxylate transporters (MCTs),^[5] predominantly MCT4, for efflux of lactate/H⁺ to maintain a stable intracellular pH and induce an

acidic tumor microenvironment. The elevated MCT4 expression has been correlated with metastasis, angiogenesis, poor prognosis, and recurrence of many cancers.^[6]

In parallel to altering the energy metabolism, hypoxia also triggers more production of reactive oxygen species (ROS; up to 100 μM) in tumor cells than normal tissues (ca. 20 nM).^[7] The elevated ROS (in particular H₂O₂) could foster tumor growth and malignant progression.^[8] On the other hand, owing to the high ROS levels, tumor cells are also more vulnerable to further oxidative assault than normal cells.^[9] The generation of more reactive and toxic ROS (such as [•]OH) caused by exogenous agents could disrupt the ROS homeostasis in tumor cells, leading to severe oxidative stress and then cell death. Therefore, we hypothesized that co-targeting of these two cancer hallmarks, aerobic glycolysis and dysregulated redox homeostasis, in tumor cells could be a novel strategy for efficiently and specifically arresting tumor progression.

Herein, we developed a unique amorphous iron oxide (AIO) RNAi NP platform (Scheme 1) for co-targeting metabolic and ROS homeostasis in tumor cells by simultaneously silencing MCT4 to induce tumor cell acidosis and exacerbating oxidative stress via the Fenton-like reaction. These NPs exhibit multiple appealing features for systemic siRNA delivery. First, different from previous iron oxide RNAi NPs, in which siRNA was simply loaded on NP surface by complexing with cationic materials,^[10] our strategy enables siRNA encapsulation within NPs. This could limit enzymatic

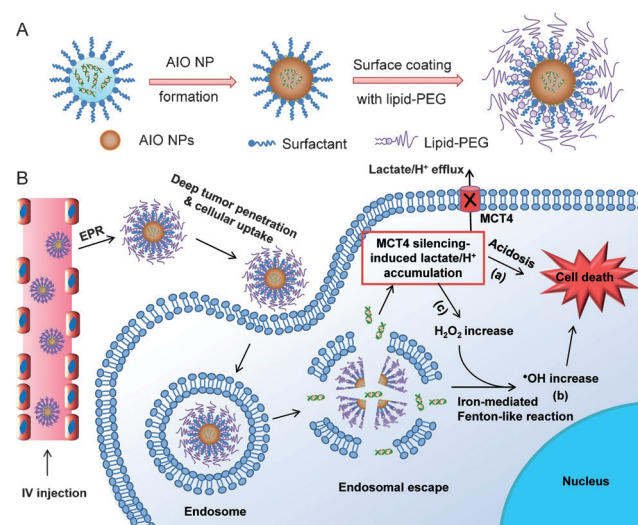
[*] Dr. Y. Liu, X. Ji, W. W. L. Tong, D. Askhatova, Dr. T. Yang, Prof. J. Shi
Center for Nanomedicine and Department of Anesthesiology
Brigham and Women’s Hospital, Harvard Medical School
Boston, MA 02115 (USA)
E-mail: ylliu@hnu.edu.cn
jshi@bwh.harvard.edu

Dr. Y. Liu
Molecular Science and Biomedicine Laboratory
State Key Laboratory of Chemo/Biosensing and Chemometrics
College of Chemistry and Chemical Engineering, Hunan University
Changsha, 410082 (P. R. China)

Dr. H. Cheng, Prof. Y. Wang
Department of Experimental Therapeutics
British Columbia Cancer Agency
Vancouver, BC, V5Z 1L3 (Canada)

Dr. T. Yang
State Key Laboratory of Biochemical Engineering
Institute of Process Engineering, Chinese Academy of Sciences
Beijing 100190 (P. R. China)

Supporting information and the ORCID identification number(s) for the author(s) of this article can be found under:
<https://doi.org/10.1002/anie.201710144>.



Scheme 1. Illustration of A) the formulation and B) multiple functions of AIO RNAi NPs.

contact, degradation, and burst release during circulation in the blood. Second, the NPs are coated with lipid-PEG for prolonged blood circulation, and show less prone to the recognition by mononuclear phagocyte system in the liver and spleen. Third, the small size (ca. 14.6 nm) could allow NPs to effectively penetrate deeply in tumor tissues. Fourth, unlike the majority of previous RNAi NPs,^[11] which utilize the cationic lipids and/or polymers to facilitate the endosomal escape, the efficient endosomal escape of our system may be attributable to osmotic pressure and/or endosomal membrane oxidation induced by the iron ions released from NPs. By the NP-mediated MCT4 silencing, the efflux of intracellular lactate/H⁺ can be blocked, leading to acidosis-induced tumor cell death (Scheme 1 B).

On the other hand, AIO NPs are responsive to acidic pHs after cellular uptake, and the released iron ions will react with H₂O₂ to generate highly reactive and toxic \cdot OH via the Fenton-like reaction.^[12] Apart from promoting the aforementioned endosomal escape, \cdot OH will drastically exacerbate oxidative stress in tumor cells and subsequently induce cell death (Scheme 1 B). Notably, the block of intracellular lactate efflux by MCT4 silencing could further stimulate more H₂O₂ production to amplify the Fenton-like reaction and oxidative damage to tumor cells for effective combinatorial therapy. Moreover, AIO NPs could be useful as a surrogate marker for real-time monitoring of biodistribution and tumor accumulation of siRNA via MRI, which will provide more insights into tumor heterogeneities and the enhanced permeability and retention (EPR) effect to identify cancer patients most likely to benefit from RNAi nanomedicines.^[13]

The RNAi NPs were first synthesized by a reversed microemulsion method (Scheme 1 A), with a siRNA encapsulation efficiency of about 50% as determined by inductively coupled plasma–mass spectrometry analysis. The average diameter of NPs was about 14.6 nm by size analysis of random 100 NPs in the transmission electron microscopy (TEM) image (Figure 1 A), and the hydrodynamic size was about 45 nm as measured by dynamic light scattering (Supporting Information, Figure S1). X-ray diffraction (XRD) confirmed the amorphous structure (Figure 1 B), which is presumably composed of Fe₂O₃ or FeOOH.^[14] To assess whether the decomposition of AIO NPs in acidic pHs can trigger \cdot OH production, we used electron spin resonance (ESR) spectroscopy to measure \cdot OH produced by the reaction between NPs and H₂O₂ at different pH values. The generation of \cdot OH was very low at pH 7.4, as indicated by the low ESR amplitude of paramagnetic adduct DEPMPO-OH (Figure 1 C). In contrast, the ESR amplitude of DEPMPO-OH was dramatically increased at pH 6.0, and further enhanced at pH 5.0, suggesting the elevated production of \cdot OH at acidic pH. AIO NPs can be decomposed at acidic pH (Supporting Information, Figure S2), thus contributing to the release of iron ions and accelerated Fenton-like reaction. Meanwhile, the NP decomposition led to fast siRNA release (Supporting Information, Figure S3).

The endosomal escape ability of AIO NPs was tested by staining endosomes with LysoTracker Green. Figure 1 D shows the effective cytosolic transport of the internalized siRNA from endosomes. Notably, the endosomal escape

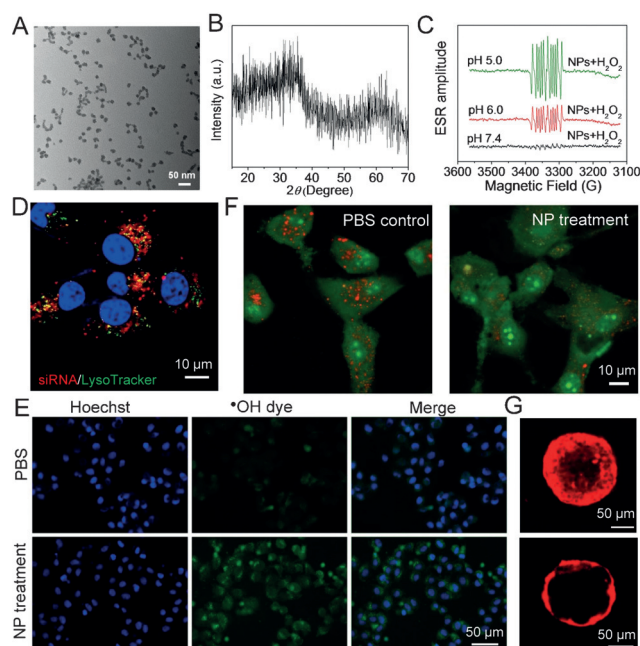


Figure 1. A) TEM image and B) XRD spectrum of AIO RNAi NPs. C) ESR spectra of AIO RNAi NPs in the presence of H₂O₂ at different pHs. 5-diethoxyphosphoryl-5-methyl-1-pyrroline N-oxide (DEPMPO) was used as the spin trap agent. D) Fluorescent image of HeLa cells treated with Cy5.5-siRNA-loaded AIO NPs for 4 h. E) Confocal imaging of intracellular \cdot OH production and F) AO staining of PC3 cells treated with PBS vs. AIO NPs. The reduced red dots in the NP-treated cells (F) indicate the loss of membrane integrity of endo/lysosomes. G) Tissue penetration of (top) AIO NPs and (down) polymer NPs loaded with Cy5.5-siRNA in a 3D spheroid model after 4 h incubation.

mechanism associated with AIO NPs may be attributable to two potential processes: 1) after internalization, AIO NPs will be dissolved at acidic endosomal pH values to release iron ions and thus increase osmotic pressure in endosomes, leading to endosomal swelling and rupture; and 2) the released iron ions can also react with intracellular H₂O₂ to generate highly reactive \cdot OH via the Fenton-like reaction, as identified by \cdot OH staining using aminophenyl fluorescein (APF; Figure 1 E). \cdot OH could then contribute to the endosomal membrane oxidation and rupture, as confirmed by staining the endosomal membrane integrity with acridine orange (AO; Figure 1 F).

Since small-size NPs have been suggested to diffuse through the tumor tissue more efficiently than large size NPs,^[15] we proceeded to evaluate the tissue penetration of AIO NPs using a 3D spheroid tumor model. As a proof-of-concept, polymer NPs with similar surface coating but with a particle size of about 100 nm were used as a reference (Supporting Information, Figure S4), given the challenge of making large AIO NPs with the reversed microemulsion method adopted in this work. Results showed that red fluorescence was observed only in the periphery of the spheroid treated with large polymer RNAi NPs, while much better tissue penetration can be seen for the group treated with AIO RNAi NPs (Figure 1 G).

Next, prostate cancer (PCa), characterized by upregulation of MCT4 and overproduction of ROS,^[16] was used as

a model to examine the combinatorial therapy of AIO RNAi NPs. The overexpression of MCT4 and the increased ROS (mainly H_2O_2) has been correlated with the cell proliferation, drug resistance, invasion, and metastasis of PCa.^[6] However, to the best of our knowledge, no study has thus far explored systemic delivery of siRNA targeting MCT4 (siMCT4) to PCa. To do this, we first examined the MCT4 expression and ROS production in three PCa cell lines including DU145, PC3, and LNCaP. All of the cells have a high expression of MCT4, while the ROS production in PC3 and LNCaP cells was higher than that in DU145 cells (Supporting Information, Figure S5). Correspondingly, the cell death in PC3 and LNCaP cells caused by AIO NP-mediated oxidative damage was more obvious than that in DU145 cells (Supporting Information, Figure S6). Thus, PC3 cells, with high ROS production and MCT4 expression, were used for the following experiments unless otherwise specified. Western blot and immunofluorescence analysis demonstrated that NP-(siMCT4) treatment significantly suppressed the expression of MCT4 in PC3 cells (Figure 2 A,B). As a result, a significant increase of the intracellular lactate was observed (Figure 2 C). Moreover, we found that the intracellular H_2O_2 production in PC3 cells was dramatically enhanced after MCT4 silencing (Figure 2 D). This may be presumably attributed to the MCT4 silencing-induced lactate accumulation, which can activate mitochondrial biogenesis via upregulation of PGC1 α and subsequently increase the intracellular H_2O_2 .^[17] The produced H_2O_2 could further react with iron ions released from AIO NPs to generate more $\cdot OH$ and thus amplify the oxidative

damage to tumor cells. Figure 2E shows that NP(siMCT4) were most effective in suppressing cell proliferation compared to the NP(siControl) or non-treated group, which was primarily due to the drastic apoptosis caused by MCT4 silencing and the amplified oxidative damage (Figure 2 F–H).

Given these promising *in vitro* results, we proceeded to examine the *in vivo* performance of AIO NPs. The pharmacokinetics and biodistribution studies were first carried out by intravenous (iv) injection of Cy5.5-siRNA-loaded AIO NPs. The AIO NPs demonstrated long circulation in the blood (Figure 3 A), effective accumulation in the tumor, and less

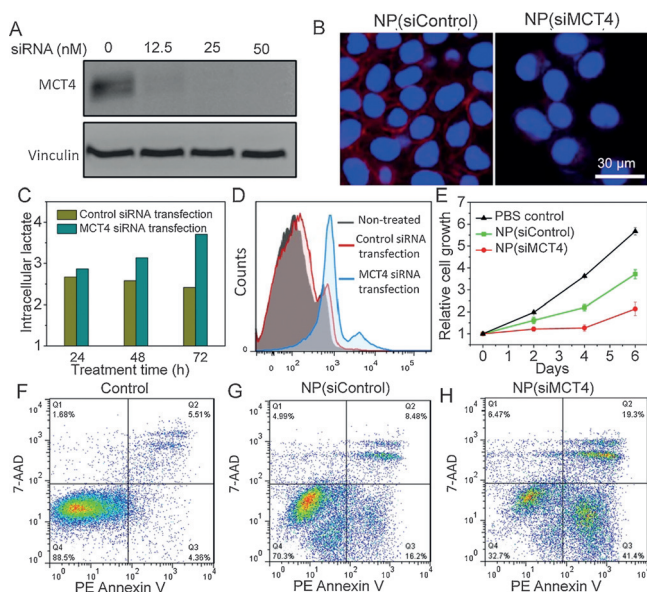


Figure 2. A) Western blot and B) immunofluorescence analysis of MCT4 expression in PC3 cells treated with NP(siControl) vs. NP-(siMCT4). C) Time-dependent intracellular lactate change in PC3 cells with vs. without MCT4 silencing. D) ROS production of PC3 cells with vs. without MCT4 silencing. Note that Lipofectamine 2000 was used for siRNA transfection in this experiment, as it will not induce Fenton-like reaction. E) Proliferation of PC3 cells treated with PBS, NP(siControl), or NP(siMCT4). F)–H) Flow cytometry analysis of PC3 cell apoptosis post treatment of (F) PBS, (G) NP(siControl), and (H) NP(siMCT4).

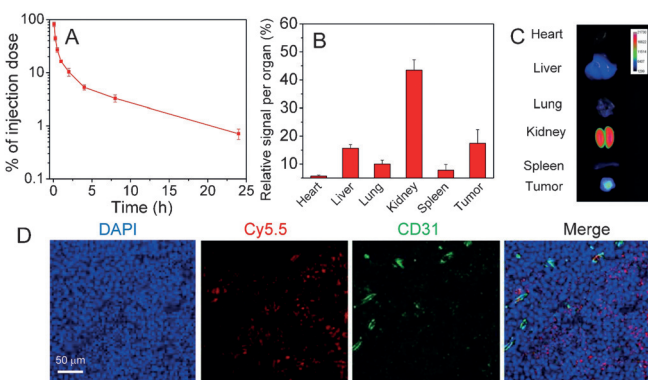


Figure 3. A) Pharmacokinetic profile and B) biodistribution of Cy5.5-siRNA-loaded AIO NPs. C) Fluorescent imaging of organs from PC3 tumor-bearing mouse at 24 h after iv injection of Cy5.5-siRNA-loaded AIO NPs. D) Fluorescent images of the tumor sections of the PC3 tumor-bearing mouse sacrificed at 4 h post-injection of Cy5.5-siRNA-loaded AIO NPs.

uptake by the liver and spleen (Figure 3 B,C). Furthermore, we also examined the *in vivo* tumor-penetrating ability of AIO NPs by immunofluorescence analysis. As shown in Figure 3 D, bright red fluorescence was visualized in the blood vessels and the extravascular tumor parenchyma, suggesting that AIO NPs could efficiently extravasate from the leaky tumor vasculature and transport deeply into the tumor tissue.

In vivo gene silencing of AIO RNAi NPs was then examined after iv injection of the NPs into PC3 tumor-bearing mice for three consecutive injections at a 900 μg siRNA/kg dose. Compared to the NP(siControl)-treated group, the MCT4 expression was significantly suppressed in mice treated with NP(siMCT4) (Figure 4 A; Supporting Information, Figure S7). Next, the *in vivo* antitumor effect of NPs was evaluated. AIO RNAi NPs were iv injected into PC3 tumor-bearing mice for four consecutive injections at a 900 μg siRNA/kg dose and the tumor growth was monitored. NP(siControl) treatment reduced the tumor growth compared to the control group owing to the Fenton-like reaction-induced oxidative damage (Figure 4 B,C). More impressively, a further suppression of tumor growth was observed for the NP(siMCT4)-treated group, without causing noticeable influence on the body weight (Supporting Information, Figure S8).

Along with combinatorial cancer therapy, noninvasive visualization of the tumor accumulation of AIO RNAi NPs could be achieved via MRI, as iron oxide NPs are well-known

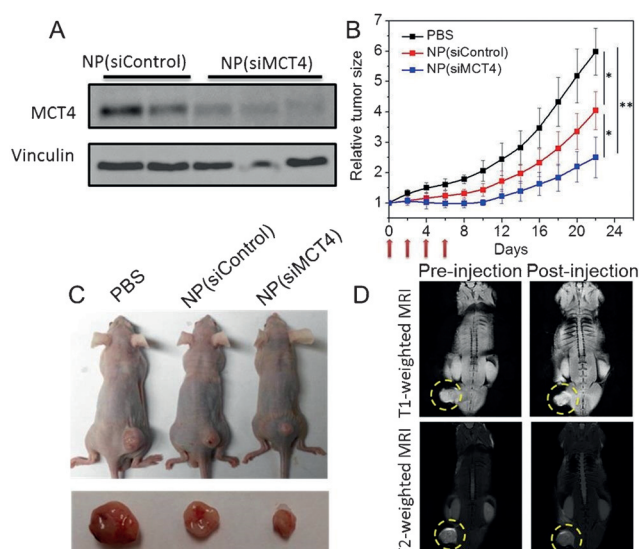


Figure 4. A) Western blot analysis of the MCT4 expression in PC3 tumor-bearing mice after iv injection of NP(siControl) vs. NP(siMCT4). B) Tumor growth of PC3 xenograft mice after treatment with PBS, NP(siControl), or NP(siMCT4). (* $p < 0.05$ and ** $p < 0.01$ vs. PBS control). C) Representative picture of tumor-bearing mice and tumor tissues from three different groups. D) Whole body T₁- and T₂-weighted MRI images of the PC3 tumor-bearing mouse after iv injection of AIO RNAi NPs.

as MRI contrast agents.^[18] Notably, unlike commercial iron oxide NPs that are generally T₂-weighted MRI contrast agents, our AIO NPs showed both T₁ and T₂ contrast effects (Supporting Information, Figure S9). The dual-model imaging effect may be presumably due to the amorphous structure and small size of AIO NPs, while further studies will still be needed to reveal the imaging mechanisms. Our preliminary data also demonstrated that the tumor accumulation of AIO NPs via the EPR effect could be visualized in both T₁- and T₂-weighted MRI images after iv injection (Figure 4D), suggesting the potential use of AIO NPs for MRI-guided siRNA delivery and the selection of patients with high EPR effect.^[13]

Finally, the potential side effects of NPs were evaluated. Systemic administration of AIO NPs did not induce obvious changes in the serum levels of multiple hematological parameters (Supporting Information, Figure S10) and cytokines (Supporting Information, Figure S11). Moreover, histological analysis shows no noticeable inflammatory response or tissue injury in the NP-treated mice, as compared to the control group (Supporting Information, Figure S12). All these results suggest the good biocompatibility of AIO NPs.

In conclusion, we developed an innovative amorphous iron oxide NP platform for effective systemic siRNA delivery, and for concurrently targeting two distinct cancer hallmarks for combinatorial therapy. The NPs exhibit several promising features, such as small size, efficient gene silencing, high tumor accumulation, deep tumor tissue penetration, good biocompatibility, and MRI-mediated tracking of tumor accumulation. We expect this unique platform to become a valuable tool for theranostic treatment of advanced cancers.

Acknowledgements

Financial support by NIH/NCI R01CA200900 and the Prostate Cancer Foundation Young Investigator Award.

Conflict of interest

The authors declare no conflict of interest.

Keywords: cancer hallmarks · iron oxide nanoparticles · MRI · RNAi · tumor penetration

How to cite: *Angew. Chem. Int. Ed.* **2018**, *57*, 1510–1513
Angew. Chem. **2018**, *130*, 1526–1529

- [1] W. R. Wilson, M. P. Hay, *Nat. Rev. Cancer* **2011**, *11*, 393.
- [2] N. C. Denko, *Nat. Rev. Cancer* **2008**, *8*, 705.
- [3] U. E. Martinez-Outschoorn, M. Peiris-Pages, R. G. Pestell, F. Sotgia, M. P. Lisanti, *Nat. Rev. Clin. Oncol.* **2017**, *14*, 113.
- [4] R. A. Cairns, I. S. Harris, T. W. Mak, *Nat. Rev. Cancer* **2011**, *11*, 85.
- [5] A. P. Halestrap, *IUBMB Life* **2012**, *64*, 1.
- [6] S. Y. Choi, H. Xue, R. Wu, L. Fazli, D. Lin, C. C. Collins, M. E. Gleave, P. W. Gout, Y. Wang, *Clin. Cancer Res.* **2016**, *22*, 2721.
- [7] a) S. S. Sabharwal, P. T. Schumacker, *Nat. Rev. Cancer* **2014**, *14*, 709; b) S. Zhai, X. Hu, Y. Hu, B. Wu, D. Xing, *Biomaterials* **2017**, *121*, 41; c) B. Halliwell, M. V. Clement, L. H. Long, *FEBS Lett.* **2000**, *486*, 10.
- [8] E. Panieri, M. M. Santoro, *Cell Death Dis.* **2016**, *7*, e2253.
- [9] M. R. Ramsey, N. E. Sharpless, *Nat. Cell Biol.* **2006**, *8*, 1213.
- [10] a) S. Jiang, A. A. Eltoukhy, K. T. Love, R. Langer, D. G. Anderson, *Nano Lett.* **2013**, *13*, 1059; b) G. Liu, J. Xie, F. Zhang, Z. Wang, K. Luo, L. Zhu, Q. Quan, G. Niu, S. Lee, H. Ai, X. Chen, *Small* **2011**, *7*, 2742; c) J. W. Park, K. H. Bae, C. Kim, T. G. Park, *Biomacromolecules* **2011**, *12*, 457.
- [11] a) R. Kanasty, J. R. Dorkin, A. Vegas, D. Anderson, *Nat. Mater.* **2013**, *12*, 967; b) Y. Liu, V. Gunda, X. Zhu, X. Xu, J. Wu, D. Askhatova, O. C. Farokhzad, S. Parangi, J. Shi, *Proc. Natl. Acad. Sci. USA* **2016**, *113*, 7750; c) J. E. Zuckerman, M. E. Davis, *Nat. Rev. Drug Discovery* **2015**, *14*, 843; d) J. Lee, P. E. Saw, V. Gujrati, Y. Lee, H. Kim, S. Kang, M. Choi, J. I. Kim, S. Jon, *Theranostics* **2016**, *6*, 192; e) Y. Wang, L. Miao, A. Satterlee, L. Huang, *Adv. Drug Delivery Rev.* **2015**, *87*, 68.
- [12] a) S. P. Foy, V. Labhasetwar, *Biomaterials* **2011**, *32*, 9155; b) A. L. Pham, F. M. Doyle, D. L. Sedlak, *Water Res.* **2012**, *46*, 6454.
- [13] J. Shi, P. W. Kantoff, R. Wooster, O. C. Farokhzad, *Nat. Rev. Cancer* **2017**, *17*, 20.
- [14] P. Leidinger, J. Treptow, K. Hagens, J. Eich, N. Zehethofer, D. Schwudke, W. Oehlmann, H. Lunsdorf, O. Goldmann, U. E. Schaible, K. E. Dittmar, C. Feldmann, *Angew. Chem. Int. Ed.* **2015**, *54*, 12597; *Angew. Chem.* **2015**, *127*, 12786.
- [15] S. Barua, S. Mitragotri, *Nano Today* **2014**, *9*, 223.
- [16] L. Marignol, K. Rivera-Figueroa, T. Lynch, D. Hollywood, *Nat. Rev. Urol.* **2013**, *10*, 405.
- [17] T. Hashimoto, R. Hussien, S. Oommen, K. Gohil, G. A. Brooks, *FASEB J.* **2007**, *21*, 2602.
- [18] J. Xie, S. Jon, *Theranostics* **2012**, *2*, 122.

Manuscript received: October 1, 2017

Revised manuscript received: December 6, 2017

Accepted manuscript online: December 24, 2017

Version of record online: January 16, 2018